Photocell Optimization Using Dark State Protection

Amir Fruchtman,[1] Rafael Gómez-Bombarelli,[2] Brendon W. Lovett,[3] and Erik M. Gauger[4,*]
[1]Department of Materials, University of Oxford, Oxford OX1 3PH, United Kingdom
[2]Department of Chemistry and Chemical Biology, Harvard University, Cambridge, Massachusetts 02138, USA
[3]SUPA, School of Physics and Astronomy, University of St. Andrews, St Andrews KY16 9SS, United Kingdom
[4]SUPA, Institute of Photonics and Quantum Sciences, Heriot-Watt University, Edinburgh EH14 4AS, United Kingdom
(Received 17 December 2015; published 10 November 2016)

Conventional photocells suffer a fundamental efficiency threshold imposed by the principle of detailed balance, reflecting the fact that good absorbers must necessarily also be fast emitters. This limitation can be overcome by "parking" the energy of an absorbed photon in a dark state which neither absorbs nor emits light. Here we argue that suitable dark states occur naturally as a consequence of the dipole-dipole interaction between two proximal optical dipoles for a wide range of realistic molecular dimers. We develop an intuitive model of a photocell comprising two light-absorbing molecules coupled to an idealized reaction center, showing asymmetric dimers are capable of providing a significant enhancement of light-to-current conversion under ambient conditions. We conclude by describing a road map for identifying suitable molecular dimers for demonstrating this effect by screening a very large set of possible candidate molecules.

DOI: 10.1103/PhysRevLett.117.203603

The operation of a solar energy harvesting device can be enhanced by clever design of a nanoscopic, quantum mechanical system [1]. Although thermodynamical considerations lead to the famous Shockley-Queisser efficiency limit for classical photocell devices [2], the "detailed balance" underlying this limit can be broken by careful use of quantum interference. In particular, by carefully tailoring the interactions between two [3,4] or more [5,6] idealized and identical two-level energy absorbers, it is possible to prevent the reemission of absorbed light by arranging that excitations end up in "dark"—i.e., optically inaccessible—states. This allows the energy to be dissipated across a target load, rather than dissipated via spontaneous emission.

It is conjectured that Nature already exploits quantum-mechanical properties in order to increase the light-harvesting efficiency of photosynthesis [7]. The most well-studied system in this context is the Fenna-Matthews-Olsen complex [8], which connects the antenna to the reaction center in the light harvesting apparatus of green sulfur bacteria. It consists of eight bacteriochlorophyll (BChl a) molecules [9] that are held in place by a messy protein scaffold, and surrounded by water at room temperature, resulting in nonidentical BChl excitation energies. True quantum effects may seem unlikely in the "hot and wet" conditions of such systems. However, the observation of quantum coherent beats in experimentally measured two-dimensional electronic spectroscopy suggests otherwise [10–16].

A good definition of the term efficiency is key to quantifying a quantum advantage. One such measure is the energy transfer efficiency, i.e., the probability of an excitation reaching the target electron acceptor after starting from a spatially localized state [17–19], but this does not capture all aspects of the process. An alternative approach is placing a system between two electrodes, and measuring the current through them [20–23]. Dorfman *et al.* proposed a different canonical measure [1]: They consider the entire cycle, from absorbing a photon to extracting work, as a quantum heat engine (QHE). Procedurally, they abstract the electron acceptor to become a two-level "trap," in which transferred electrons "fill" the excited state before the action of driving a load resistor is mimicked by decay to the lower level of the trap. This gives a straightforward way of defining the power and the efficiency of the heat engine. In this picture, Fano interference may boost the photocurrent by 27% over that of a classical cell. Subsequently, Creatore *et al.* [3] reported an efficiency gain of 35% by introducing the different effect of *dark-state protection* using two identical dipole-coupled emitters. Further gains become possible for more than two chromophores [5,6].

In this Letter, we use the QHE framework to determine whether a quantum advantage is achievable in nonidealized situations typical of real devices and conditions more closely resembling the photosynthetic apparatus. In particular, we consider a light harvesting device where the two constituent chromophores are not identical. Surprisingly, we will find that under realistic constraints an "asymmetric" dimer may even significantly outperform previously studied systems. Presenting several example molecules that would be highly efficient light harvesters according to our model, we argue that the number of conceivable molecular dimers with a quantum advantage is vast.

We now introduce a general framework that will allow us to define three specific models shortly. We consider two, generally different, light-absorbing molecules with dipolar coupling (Fig. 1). There is a further coupling to an abstracted reaction center trap, modeled as a two-level system $|\alpha\rangle$, $|\beta\rangle$ with corresponding energies ϵ_α, ϵ_β, following Ref. [1]. An excitation absorbed by the molecules can be incoherently transferred into the reaction center via a phonon-assisted process. In what follows we restrict the dynamics to the subspace with one or zero excitations across the entire system: this approximation is valid since in realistic configurations inspired by natural photosynthetic systems, the average excitation number is very small ($N \approx 0.02$ for an energy gap of 2 eV and sunlight temperature of 6000 K). Since photoexcitation is very rare, once captured it is paramount to preventing spontaneous emission back into the environment. Hence, access to a dark state, i.e., a state that is decoupled from the photon field and thus not susceptible to spontaneous emission decay, can enhance the engine's efficiency. By Kasha's rule reemission of absorbed photons will be dominated by the lowest excited state, motivating our approach of only considering a single excited level per chromophore.

We denote the excited states in the molecules as $|1\rangle, |2\rangle$ with energies ϵ_1, ϵ_2, respectively, and the ground state as $|g\rangle$ with energy ϵ_g, and J_{12} is the dipolar coupling between the molecules. The Hamiltonian of the system is thus of dimension five and given by (see Fig. 2)

$$\mathcal{H}_s = \epsilon_1|1\rangle\langle 1| + \epsilon_2|2\rangle\langle 2| + \epsilon_g|g\rangle\langle g| + \frac{J_{12}}{2}(|1\rangle\langle 2| + |2\rangle\langle 1|) + \epsilon_\alpha|\alpha\rangle\langle\alpha| + \epsilon_\beta|\beta\rangle\langle\beta| \quad (1)$$

$$= \epsilon_+|+\rangle\langle +| + \epsilon_-|-\rangle\langle -| + \epsilon_g|g\rangle\langle g| + \epsilon_\alpha|\alpha\rangle\langle\alpha| + \epsilon_\beta|\beta\rangle\langle\beta|. \quad (2)$$

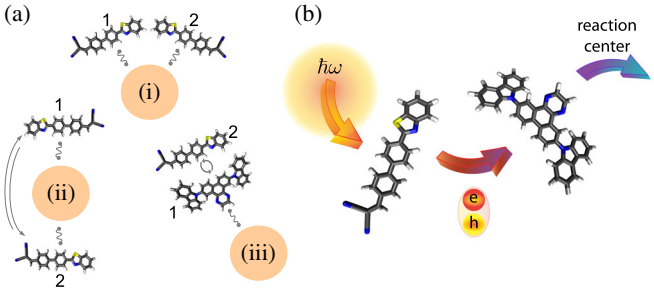

FIG. 1. (a) Schematic of the different models: (i) independent, (ii) symmetric, and (iii) asymmetric, depicted with molecules from row F in Table S1 [24]. (In)coherent coupling is denoted by (wiggly) rounded arrows and the circle denotes the reaction center. (b) Energy flow through asymmetric model: the donor chromophore with strong optical oscillator strength absorbs a photon and transfers it to its darker partner via Förster transfer. Delocalization across the dimer of the relevant quantum eigenstates is not depicted.

In the second equation, $|\pm\rangle$ are the usual eigenstates diagonalizing the subspace spanned by $|1\rangle, |2\rangle$.

In addition to the bare system we also have the solar photonic bath at $T_h = 6000$ K, which can induce spontaneous and stimulated transitions $|1\rangle \leftrightarrow |g\rangle$ and $|2\rangle \leftrightarrow |g\rangle$. Further, each molecule is embedded in its own local environment of vibrational modes, treated as infinite phonon baths at room temperature $T_c = 300$ K. A generic spin boson type interaction between excitonic states and phonon modes yields transitions between the energy eigenstates $|+\rangle \leftrightarrow |-\rangle, |+\rangle \leftrightarrow |\alpha\rangle, |-\rangle \leftrightarrow |\alpha\rangle, |\beta\rangle \leftrightarrow |g\rangle$ [31]. Further, we include the reaction center decay with rate $\gamma_{\alpha\beta}$, and some leakage between $|\alpha\rangle$ and $|g\rangle$ with rate $\chi\gamma_{\alpha\beta}$. The interaction Hamiltonian is thus

$$\mathcal{H}_I = \hat{I}_{1g} + \hat{I}_{2g} + \hat{I}_{11} + \hat{I}_{22} + \hat{I}_{1\alpha} + \hat{I}_{2\alpha} + \hat{I}_{\beta g}. \quad (3)$$

Here $\hat{I}_{ab} = \frac{1}{2}(|a\rangle\langle b| + |b\rangle\langle a|)\hat{\mu}_{ab}$, and $\hat{\mu}$ are operators of the coupling to the different environments: $\hat{\mu}_{1g}$, $\hat{\mu}_{2g}$ are dipole operators, and the rest are phonon operators [24].

Applying a standard Born-Markov procedure [32] we arrive at a set of Pauli master equations [24]:

$$\frac{\partial}{\partial t}\vec{P} = \mathcal{Q}\vec{P}. \quad (4)$$

Here $\vec{P} = \{P_+, P_-, P_\alpha, P_\beta, P_g\}^\dagger$ is a vector of the populations in the diagonal basis of the system, and $\mathcal{Q}$ is a matrix of the different rates, respecting detailed balance for photon and phonon baths independently. Resulting transition rates are depicted in Fig. 2 and conservation of total population imposes the additional constraint $\sum_i P_i = 1$. We give the explicit entries of $\mathcal{Q}$ in the Supplemental Material (SI) [24], and also show that this rate equation approach is valid by direct comparison with the full Bloch-Redfield equations.

Utilising the concept of a photochemical voltage [33], we attribute an effective current and voltage to the reaction center [1]:

$$I = e\gamma_{\alpha\beta}P_\alpha, \qquad V = \epsilon_\alpha - \epsilon_\beta - k_B T_c \ln(P_\alpha/P_\beta). \quad (5)$$

Following Refs. [1,3–5,34] we now consider quantity $P = IV$ as a measure of the power generated by the system.

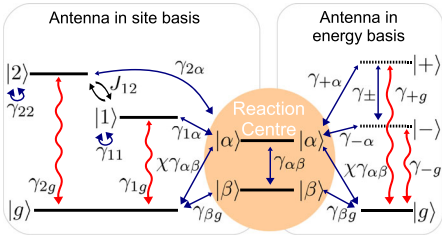

FIG. 2. Level structure schematic of the three models. On the left we show the system in the site basis and on the right in the energy basis. The reaction center is the same in both. We denote radiative transitions by wiggly red arrows, and nonradiative phonon-induced transitions by blue arrows.

Here T_c is the (cold) phonon temperature, k_B the Boltzmann constant, and e the electron charge. In the absence of sunlight, the system thermalizes to the phonon bath temperature, and the voltage vanishes. Thus V is a measure of the deviation from the thermal state with temperature T_c. We are interested in the steady-state power output, which is found by setting the left-hand side of Eq. (4) to zero and solving the resulting simultaneous algebraic equations.

Our Hamiltonian is static, and so there is no cycle as there would be for conventional quantum heat engines [35–37]; our device rather relies on heat flowing through the reaction center to produce work [38–40]. Henceforth, we adopt the maximal achievable steady state power as our measure of efficiency: we treat the reaction center as a black box optimizing its $\gamma_{\alpha\beta}$ to generate maximal power (keeping all other parameters fixed). For a representative example of the behavior of P and I as a function of V see Fig. S5 [24].

We now define the three specific models which we shall compare. These have contrasting molecular geometries and are depicted in Fig. 1. First, the *independent model* has two identical light harvesting molecules that are not directly coupled to one another while each is independently coupled to the reaction center. Specifically $\hat{\mu}_{1g} = \hat{\mu}_{2g}$; $\hat{\mu}_{1\alpha}$, $\hat{\mu}_{2\alpha}$ represent the coupling to different phonon baths, and $J_{12} = \gamma_{+-} = 0$. Further, we let $\gamma_{+g} = \gamma_{-g}$, $\gamma_{+\alpha} = \gamma_{-\alpha}$, $\epsilon_+ = \epsilon_-$. This model does not exhibit dark state protection and serves as a benchmark for the other models.

Second, the *symmetric model* mirrors that described in Ref. [3] and consists of two identical, directly coupled molecules: $\epsilon_1 = \epsilon_2$, $\hat{\mu}_{1g} = \hat{\mu}_{2g}$, and $J_{12} > 0$. This arrangement leads to a dark and bright state, $|+\rangle$ and $|-\rangle$ respectively, with $\gamma_{-g} = 0$ and $\gamma_{+-} = \frac{1}{4}(\gamma_{11} + \gamma_{22})$. The molecules couple to the reaction center in antiphase $\hat{\mu}_{1\alpha} = -\hat{\mu}_{2\alpha}$ [3], rendering $\gamma_{+\alpha} = 0$. We discuss deviations from this idealized scenario in the SI [24].

Finally, the *asymmetric model* is the main focus of our Letter. It comprises two nonidentical molecules $\epsilon_1 < \epsilon_2$ with different dipole moments $\hat{\mu}_{1g} = z\hat{\mu}_{2g}$ where $z < 1$ represents the asymmetry. The dark(er) $|-\rangle$ state has a larger overlap with molecule 1, which we imagine closer to the reaction center, and we assume molecule 2 only has negligibly small reaction center coupling ($\hat{\mu}_{2\alpha} = 0$). We believe that this configuration should be easier to realize than the symmetric model, while allowing engineering of the energy gap $\epsilon_+ - \epsilon_-$. For flat spectral densities of the environments around the transition frequencies, we find this asymmetric model exhibits a fully dark state, provided that J_{12}, z, and $\epsilon_2 - \epsilon_1$ satisfy the relation:

$$J_{12} = \frac{2z}{1 - z^2}(\epsilon_2 - \epsilon_1). \tag{6}$$

Explicit rates for this system are given in the SI [24]. Whether or not $|-\rangle$ is indeed fully dark, we can express the resulting total excitation rate through an angle Φ:

$$\gamma_{+g} = (\gamma_{1g} + \gamma_{2g})\cos^2\Phi, \tag{7}$$

$$\gamma_{-g} = (\gamma_{1g} + \gamma_{2g})\sin^2\Phi. \tag{8}$$

Thus $\tan^2\Phi = \gamma_{-g}/\gamma_{+g}$, and $\tan^2\Phi = 0$ in the presence of a completely dark state.

Several mechanisms may cause deviation from a fully dark state in both coupled models: First, different local environments would generally entail differing reorganization energy shifts and thus excitation energies. For example, the Fenna-Matthews-Olsen complex consists of eight identical BChl units, embedded in a protein scaffolding, resulting in on-site energies spanning a range of 25 meV [10]. Second, the two dipoles may be at an angle φ instead of parallel [3], breaking the interference needed for a completely dark state. Third, the coherent coupling J_{12} depends on both the distance between the two molecules, and the angle φ: $J_{12} = J_{12}^0 \cos\varphi$, where J_{12}^0 is the coupling with parallel dipoles. Taking all this into account we get in the general case, i.e., for all models,

$$\tan^2\Phi = \frac{\Omega_R(1+z^2) - (\epsilon_2 - \epsilon_1)(1-z^2) - 2zJ_{12}\cos\varphi}{\Omega_R(1+z^2) + (\epsilon_2 - \epsilon_1)(1-z^2) + 2zJ_{12}\cos\varphi}, \tag{9}$$

with $\Omega_R = \sqrt{(\epsilon_2 - \epsilon_1)^2 + J_{12}^2}$ being the Rabi frequency of the bare system between sites 1 and 2. Further discussion about deviation from the fully dark state, and details on the coupling to the reaction center are given in the SI [24].

The performance of the (a)symmetric relative to the independent models will be assessed by using our simulations to determine the ratio of the respective maximum powers, found by varying $\gamma_{\alpha\beta}$ in each case [see Eq. (5)]. For a fair comparison, we keep $\gamma_{+g} + \gamma_{-g}$, ϵ_-, and $\gamma_{1\alpha}$ equal across all three models.

Figure 3 presents the enhancement achievable by dark-state protection. Here we have optimized J_{12} as well as $\gamma_{\alpha\beta}$

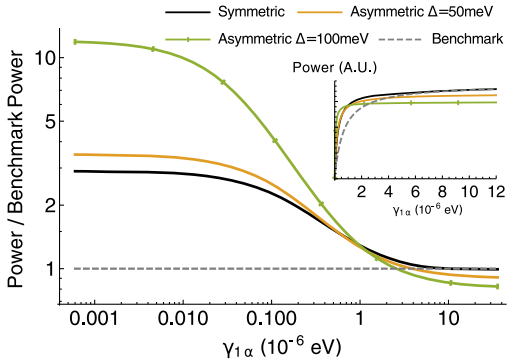

FIG. 3. Power enhancement over the benchmark achievable through a dark state, as a function of the trapping rate on a log-log scale. The parameters were chosen to enable comparison with Ref. [3]: $\gamma_{1g} + \gamma_{2g} = 1.24 \times 10^{-6}$ eV, $\gamma_{11} = \gamma_{22} = 0.005$ eV, $\gamma_{\beta g} = 0.0248$ eV, $T_h = 6000$ K, $T_c = 300$ K, $\epsilon_- = 2$ eV, $\epsilon_\alpha = 1.8$ eV, $\epsilon_\beta = 0.2$ eV, $\chi = 0.2$. Inset: the total power output of the systems in arbitrary units.

with all other parameters fixed. We also constrain J_{12} to below 30 meV as an upper limit of realistic coupling strength. For the asymmetric model the dark state criterion, Eq. (6), informs an appropriate dipole asymmetry z for a given value of J_{12}. Quantum enhancement is only possible when the transfer into the reaction center is relatively slow and constitutes a bottleneck in the cycle. In the limit of $\gamma_{1\alpha} \to 0$ an upper bound to the enhancement emerges. Within a reasonable parameter range this limit grows with increasing J_{12} for the symmetric and with $\epsilon_2 - \epsilon_1$ for the asymmetric case. As strong coupling is more difficult to realize than site energy mismatch, asymmetric dimers might more easily achieve high performance. We note that deeper into the slow transfer limit the potential enhancement factors can significantly exceed the values of up to 50% reported by Refs. [1,3,5]. By contrast, for fast transfer rates dark-state protection offers no advantage: absorbing photons at an energy higher than the extraction energy (i.e., at reduced thermal photon occupancy), combined with $\gamma_{2\alpha} = 0$, is now detrimental.

Figure 4 shows the relative power enhancements of the asymmetric model as a function of the energy difference $\epsilon_1 - \epsilon_2$ and of the coupling J_{12}. We also plot the equivalent enhancement given by the symmetric model, and show there is a parameter regime, with boundaries marked by a black line, for which the asymmetric model outperforms the symmetric one. The asymmetric model displays a peak power enhancement at finite coupling and energy difference. This happens for two reasons: First, in the regime $\epsilon_+ - \epsilon_- \lesssim k_B T$, the rate $|-\rangle \to |+\rangle$ is non-negligible, and so the dark state is not protected. Second, if $\epsilon_+ - \epsilon_- \gg J_{12}$, the rate $|+\rangle \to |-\rangle$ becomes negligible, and the dark state is rarely populated. Note that in the limit $J_{12} \to 0$, the asymmetric model gives a smaller power than the independent benchmark. This is because we set $\gamma_{2\alpha} = 0$ for the asymmetric model, effectively making it a single antenna setup benchmarked against two antennae. We examine further realistic imperfections, including the presence of additional dephasing mechanisms, in the SI [24].

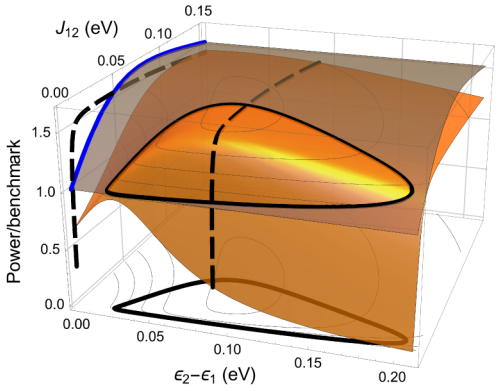

FIG. 4. Orange surface: relative power enhancement of the asymmetric model, as a function of the energy difference $\epsilon_2 - \epsilon_1$ and coupling J_{12}. Gray surface: relative power enhancement of the symmetric model (independent of $\epsilon_2 - \epsilon_1$). Black dashed line: asymmetric model enhancement for a fixed $\epsilon_2 - \epsilon_1 = 90$ meV. The dashed line is projected onto the $\epsilon_2 - \epsilon_1 = 0$ plane, for comparison with the symmetric equivalent (solid blue). The black thick line is the contour where the symmetric and asymmetric power ratios are equal. Parameters are as in Fig. 3 and with $\gamma_{1\alpha} = 6 \times 10^{-7}$ eV.

To assess the feasibility of generating suitable asymmetric molecules for power enhancement, we use a library containing quantum-chemically predicted properties of organic light-emitting diode molecules [41] to identify systems that minimize $\tan^2\Phi$ in Eq. (9). The SI [24] provides a full account of how quantum chemical calculations lead to promising molecular dimer candidates through a rigorous multistage process. Our donor candidates feature strongly allowed optical transitions (μ of 3.5 atomic units) and site energies between 3.5 to 2.5 eV to optimally absorb sunlight. As required by the model, acceptable acceptor compounds must have $\epsilon_1 < \epsilon_2$ and possess lower transition dipole moments with $z \approx 0.2$ to deliver $\tan^2\Phi \lesssim 0.05$. For simplicity, we assume fully aligned transition dipole moments and center-to-center distances between donor and acceptor moieties of 1 nm (approximately corresponding to the size of a small aromatic bridging group), resulting in an intersite coupling of up to 15 meV. Importantly, we analyze the properties of our dimers in both ground and excited state equilibrium geometry to identify systems whose relevant properties are robust to vibrational relaxation effects accompanying optical absorption and emission.

The predicted properties of a selection of molecular pairs are reported in Table S1 [24] and an illustration of some molecules is shown in Fig. S1 [24]. These examples provide evidence that the chemical regime required for dark-state protection is readily available in ordinary molecular systems. A full implementation of the proposed model would also require an additional molecular system to act as a trap, as well as control over orientation and distance between donor and acceptor. Whereas the chemical synthesis of such a complex structure is challenging, our results show that matching fundamental components for such a system is entirely feasible.

In conclusion, we have presented a general model of light absorption by an asymmetric pair of coupled chromophores, finding that it can outperform both the symmetric dimer and a pair of independent molecules in realistic parameter regimes of operation for a solar cell device. Not relying on identically matched coupled chromophores, this approach is more robust to deviations from the delicate conditions required by its symmetric counterpart. Moreover, we have shown that an abundance of real pairs of molecules have the required asymmetric properties, and indeed, such asymmetry is an integral part of natural photosynthetic systems.

The reason our asymmetric model works so well is that it enables arbitrarily large energy gaps between the bright and dark states, thus preventing phonon-assisted promotion from the dark to the bright state. In the regime where excitations are rare and the transfer into the reaction center is very slow, this translates into better protection of the excitations, thus increasing the overall efficiency of the device.

The research data supporting this publication are available online [42].

We thank Alex Chin, Ahsan Nazir, Simon Benjamin, Alán Aspuru-Guzik, and Jorge Aguilera-Iparraguirre for stimulating discussions. This work was supported by the Leverhulme Trust (RPG-080). E. M. G. is supported by the Royal Society of Edinburgh/Scottish Government. R. G. B. thanks Samsung Advanced Institute of Technology for funding. A. F. thanks the Anglo-Israel association and the Anglo-Jewish association for funding.

*e.gauger@hw.ac.uk

[1] K. E Dorfman, D. V. Voronine, S. Mukamel, and M. O. Scully, Photosynthetic reaction center as a quantum heat engine, Proc. Natl. Acad. Sci. U.S.A. **110**, 2746 (2013).

[2] W. Shockley and H. J. Queisser, Detailed balance limit of efficiency of p-n junction solar cells, J. Appl. Phys. **32**, 510 (1961).

[3] C. Creatore, M. A. Parker, S. Emmott, and A. W. Chin, Efficient Biologically Inspired Photocell Enhanced by Delocalized Quantum States, Phys. Rev. Lett. **111**, 253601 (2013).

[4] N. Killoran, S. F. Huelga, and M. B. Plenio, Enhancing light-harvesting power with coherent vibrational interactions: A quantum heat engine picture, J. Chem. Phys. **143**, 155102 (2015).

[5] Y. Zhang, S. Oh, F. H. Alharbi, G. S. Engel, and S. Kais, Delocalized quantum states enhance photocell efficiency, Phys. Chem. Chem. Phys. **17**, 5743 (2015).

[6] K. D. B. Higgins, B. W. Lovett, and E. M. Gauger, Quantum-enhanced capture of photons using optical ratchet states, arXiv:1504.05849v1.

[7] K. Mukai, S. Abe, and H. Sumi, Theory of rapid excitation-energy transfer from B800 to optically-forbidden exciton states of B850 in the antenna system LH2 of photosynthetic purple bacteria, J. Phys. Chem. B **103**, 6096 (1999).

[8] R. E. Fenna and B. W. Matthews, Chlorophyll arrangement in a bacteriochlorophyll protein from Chlorobium limicola, Nature (London) **258**, 573 (1975).

[9] J. Moix, J. Wu, P. Huo, D. Coker, and J. Cao, Efficient energy transfer in light-harvesting systems, III: The influence of the eighth bacteriochlorophyll on the dynamics and efficiency in FMO, J. Phys. Chem. Lett. **2**, 3045 (2011).

[10] J. Adolphs and T. Renger, How proteins trigger excitation energy transfer in the FMO complex of green sulfur bacteria, Biophys. J. **91**, 2778 (2006).

[11] A. Ishizaki and G. R. Fleming, Theoretical examination of quantum coherence in a photosynthetic system at physiological temperature, Proc. Natl. Acad. Sci. U.S.A. **106**, 17255 (2009).

[12] G. S. Engel, T. R. Calhoun, E. L. Read, T.-K. Ahn, T. Mancal, Y.-C. Cheng, R. E. Blankenship, and G. R. Fleming, Evidence for wavelike energy transfer through quantum coherence in photosynthetic systems. Nature (London) **446**, 782 (2007).

[13] G. Panitchayangkoon, D. Hayes, K. A. Fransted, J. R. Caram, E. Harel, J. Wen, R. E. Blankenship, and G. S. Engel, Long-lived quantum coherence in photosynthetic complexes at physiological temperature. Proc. Natl. Acad. Sci. U.S.A. **107**, 12766 (2010).

[14] Y.-C. Cheng and G. R. Fleming, Dynamics of light harvesting in photosynthesis. Annu. Rev. Phys. Chem. **60**, 241 (2009).

[15] C. Kreisbeck and T. Kramer, Long-lived electronic coherence in dissipative exciton dynamics of light-harvesting complexes, J. Phys. Chem. Lett. **3**, 2828 (2012).

[16] N. Lambert, Y.-N. Chen, Y.-C. Cheng, C.-M. Li, G.-Y. Chen, and F. Nori, Quantum biology, Nat. Phys. **9**, 10 (2012).

[17] T. Ritz, S. Park, and K. Schulten, Kinetics of excitation migration and trapping in the photosynthetic unit of purple bacteria, J. Phys. Chem. B **105**, 8259 (2001).

[18] A. Olaya-Castro, C. F. Lee, F. F. Olsen, and N. F. Johnson, Efficiency of energy transfer in a light-harvesting system under quantum coherence, Phys. Rev. B **78**, 085115 (2008).

[19] A. Shabani, M. Mohseni, H. Rabitz, and S. Lloyd, Efficient estimation of energy transfer efficiency in light-harvesting complexes, Phys. Rev. E **86**, 011915 (2012).

[20] A. Y. Smirnov, L. G. Mourokh, P. K. Ghosh, and F. Nori, High-efficiency energy conversion in a molecular triad connected to conducting leads, J. Phys. Chem. C **113**, 21218 (2009).

[21] M. Einax, M. Dierl, and A. Nitzan, Heterojunction organic photovoltaic cells as molecular heat engines: A simple model for the performance analysis, J. Phys. Chem. C **115**, 21396 (2011).

[22] M. Einax, M. Dierl, P. R. Schiff, and A. Nitzan, Multiple state representation scheme for organic bulk heterojunction solar cells: A novel analysis perspective, Europhys. Lett. **104**, 40002 (2013).

[23] S. Ajisaka, B. Žunkovič, and Y. Dubi, The molecular photocell: Quantum transport and energy conversion at strong non-equilibrium, Sci. Rep. **5**, 8312 (2015).

[24] See Supplemental Material at http://link.aps.org/supplemental/10.1103/PhysRevLett.117.203603, which includes Refs. [25–30], for more detail on the quantum chemical approach, the theoretical model, and various imperfections.

[25] R. W. Munn and R. Silbey, Theory of electronic transport in molecular crystals. II. Zeroth order states incorporating nonlocal linear electron–phonon coupling, J. Chem. Phys. **83**, 1843 (1985).

[26] R. W. Munn and R. Silbey, Theory of electronic transport in molecular crystals. III. Diffusion coefficient incorporating nonlocal linear electron–phonon coupling, J. Chem. Phys. **83**, 1854 (1985).

[27] Y. Zhao, D. W. Brown, and K. Lindenberg, On the Munn-Silbey approach to nonlocal exciton-phonon coupling, J. Chem. Phys. **100**, 2335 (1994).

[28] S. Mukamel and D. Abramavicius, Many-body approaches for simulating coherent nonlinear spectroscopies of

electronic and vibrational excitons, Chem. Rev. **104**, 2073 (2004).
[29] P. Rebentrost, M. Mohseni, and A. Aspuru-Guzik, Role of quantum coherence and environmental fluctuations in chromophoric energy transport, J. Phys. Chem. B **113**, 9942 (2009).
[30] P. Rebentrost, M. Mohseni, I. Kassal, S. Lloyd, and A. Aspuru-Guzik, Environment-assisted quantum transport, New J. Phys. **11**, 033003 (2009).
[31] Erik M. Gauger and J. Wabnig, Heat pumping with optically driven excitons, Phys. Rev. B **82**, 073301 (2010).
[32] H. P. Breuer and F. Petruccione, *The Theory of Open Quantum Systems* (Oxford University Press, New York, 2007).
[33] R. T. Ross, Some thermodynamics of photochemical systems, J. Chem. Phys. **46**, 4590 (1967).
[34] R. Stones, H. Hossein-Nejad, R. van Grondelle, and A. Olaya-Castro, How a structured vibrational environment controls the performance of a photosystem II reaction center-based photocell, arXiv:1601.05260.
[35] W. Niedenzu, D. Gelbwaser-Klimovsky, and G. Kurizki, Performance limits of multilevel and multipartite quantum heat machines, Phys. Rev. E **92**, 042123 (2015).
[36] R. Uzdin, A. Levy, and R. Kosloff, Equivalence of Quantum Heat Machines, and Quantum-Thermodynamic Signatures, Phys. Rev. X **5**, 031044 (2015).
[37] D. Gelbwaser-Klimovsky, W. Niedenzu, and G. Kurizki, *Thermodynamics of Quantum Systems under Dynamical Control* (Academic Press, 2015), Chap. 12, pp. 329–407.
[38] E. A. Martinez and J. P. Paz, Dynamics and Thermodynamics of Linear Quantum Open Systems, Phys. Rev. Lett. **110**, 130406 (2013).
[39] R. Kosloff and A. Levy, Quantum heat engines and refrigerators: Continuous devices, Annu. Rev. Phys. Chem. **65**, 365 (2014).
[40] A. Levy and R. Kosloff, The local approach to quantum transport may violate the second law of thermodynamics, Europhys. Lett. **107**, 20004 (2014).
[41] R. Gómez-Bombarelli *et al.*, Design of efficient molecular organic light-emitting diodes by a high-throughput virtual screening and experimental approach, Nat. Mater. **15**, 1120 (2016).
[42] DOI: http://dx.doi.org/10.17630/e901ecd8-e8d0-4062-a5b1-2ce2bfa5c09c.